Article

Electronic Structure Description of the *cis*-MoOS Unit in Models for Molybdenum Hydroxylases

Christian J. Doonan, Nick D. Rubie, Katrina Peariso, Hugh H. Harris, Sushilla Z. Knottenbelt, Graham N. George, Charles G. Young, and Martin L. Kirk

J. Am. Chem. Soc., **2008**, 130 (1), 55-65 • DOI: 10.1021/ja068512m

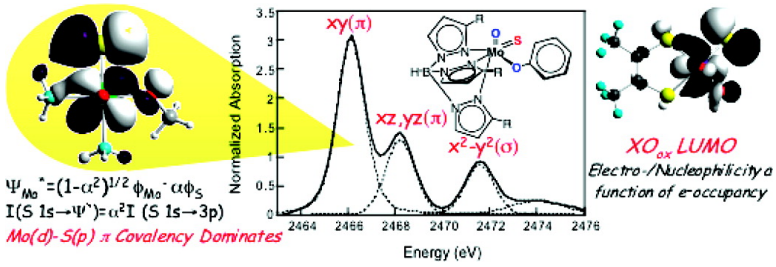

More About This Article

Additional resources and features associated with this article are available within the HTML version:

- Supporting Information
- Links to the 2 articles that cite this article, as of the time of this article download
- Access to high resolution figures
- Links to articles and content related to this article
- Copyright permission to reproduce figures and/or text from this article

View the Full Text HTML

J|A|C|S
ARTICLES
Published on Web 12/07/2007

Electronic Structure Description of the *cis*-MoOS Unit in Models for Molybdenum Hydroxylases

Christian J. Doonan,[‡] Nick D. Rubie,[†] Katrina Peariso,[†] Hugh H. Harris,[§] Sushilla Z. Knottenbelt,[†] Graham N. George,[§,⊥] Charles G. Young,*[,‡] and Martin L. Kirk*[,†]

Contribution from The Department of Chemistry and Biological Chemistry, The University of New Mexico, MSC03 20601 University of New Mexico, Albuquerque, New Mexico 87131-0001, School of Chemistry, University of Melbourne, Victoria 3010, Australia, and Stanford Synchrotron Radiation Laboratory, SLAC Stanford University, P.O. Box 4349, MS 69 Stanford, California 94309

Received November 27, 2006; E-mail: cgyoung@unimelb.edu.au; mkirk@unm.edu

Abstract: The molybdenum hydroxylases catalyze the oxidation of numerous aromatic heterocycles and simple organics and, unlike other hydroxylases, utilize water as the source of oxygen incorporated into the product. The electronic structures of the *cis*-MoOS units in $CoCp_2[Tp^{iPr}Mo^{V}OS(OPh)]$ and $Tp^{iPr}Mo^{VI}OS(OPh)$ (Tp^{iPr} = hydrotris(3-isopropylpyrazol-1-yl)borate), new models for molybdenum hydroxylases, have been studied in detail using S K-edge X-ray absorption spectroscopy, vibrational spectroscopy, and detailed bonding calculations. The results show a highly delocalized Mo=S π^* LUMO redox orbital that is formally Mo(d_{xy}) with ~35% sulfido ligand character. Vibrational spectroscopy has been used to quantitate Mo−$S_{sulfido}$ bond order changes in the *cis*-MoOS units as a function of redox state. Results support a redox active molecular orbital that has a profound influence on MoOS bonding through changes to the relative electro/nucleophilicity of the terminal sulfido ligand accompanying oxidation state changes. The bonding description for these model *cis*-MoOS systems supports enzyme mechanisms that are under orbital control and dominantly influenced by the unique electronic structure of the *cis*-MoOS site. The electronic structure of the oxidized enzyme site is postulated to play a role in polarizing a substrate carbon center for nucleophilic attack by metal activated water and acting as an electron sink in the two-electron oxidation of substrates.

Introduction

Unlike metalloenzymes which catalyze hydroxylation reactions with concomitant reduction of dioxygen, members of the xanthine oxidase (XnO) family of pyranopterin molybdenum enzymes generate, rather than consume, reducing equivalents in the oxidation of substrates.[1,2] Mammalian XnO catalyzes the final two steps of purine catabolism via the hydroxylation of hypoxanthine to xanthine and of xanthine to uric acid. The structurally related aldehyde oxidoreductases (AO) are involved in the biosynthetic pathways of retinoic acid and various phytohormones including indole-3-acetic acid and abscissic acid.[3−6] Recently, XnO and AO have been shown to oxidize 6-deoxypenciclovir, a metabolite of famciclovir, to penciclovir, which is a powerful antiviral compound.[6−9] Additionally, a number of enzymes of the XnO family have now been implicated in the activation of pro-drugs based on various synthetic guanine derivatives.[7−9] The physiological importance of these unique enzymes underscores the need to further understand their mechanism of action and how their unique active site composition, geometry, and electronic structure facilitates catalysis.[6]

The oxidized active sites of XnO and AO possess a unique *cis*-$[MoOS]^{2+}$ center (Figure 1).[10,11] Following substrate oxidation, the active site is reduced to an $[Mo^{IV}O(SH)]^{+}$ site, where molybdenum has been reduced by two electrons and the terminal sulfido has been converted to a sulfhydryl ligand (Figure 1). Although there is evidence that the sulfhydryl hydrogen is derived from the hydroxylated C−H group,[12] the description of the C−H bond scission[13] as homo- or heterolytic is still under

[†] The University of New Mexico.
[‡] University of Melbourne.
[§] Stanford Synchrotron Radiation Laboratory.
[⊥] Current address: Department of Geological Sciences, University of Saskatchewan, Saskatoon, Saskatchewan S7N 5E2, Canada.

(1) Okamoto, K.; Matsumoto, K.; Hille, R.; Eger, B. T.; Pai, E. F.; Nishino, T. *Proc. Nat. Acad. Sci. U.S.A.* **2004**, *101*, 7931−7936.
(2) Murray, K. N.; Watson, J. G.; Chaykin, S. *J. Biol. Chem.* **1966**, *241*, 4798−4801.
(3) Garattini, E.; Mendel, R.; Romao, M. J.; Wright, R.; Terao, M. *Biochem. J.* **2003**, *372*, 15−32.
(4) Krenitsky, T. A.; Neil, S. M.; Elion, G. B.; Hitchings, G. H. *Arch. Biochem. Biophys.* **1972**, *150*, 585−589.
(5) Mendel, R. R.; Hansch, R. *J. Exp. Bot.* **2002**, *53*, 1689−1698.
(6) Young, C. G. Molybdenum: MPT Enzymes. In *Encyclopedia of Inorganic Chemistry 2*; King, R. B., Ed.; Wiley: New York, 2005; Vol. V, pp 3321−3340.
(7) Clarke, S. E.; Harrell, A. W.; Chenery, R. J. *Drug Metab. Dispos.* **1995**, *23*, 251−254.
(8) Hodge, R. A. *Antiviral Chem. Chemother.* **1993**, *4*, 67−84.
(9) Rashidi, M. R.; Smith, J. A.; Clarke, S. E.; Beedham, C. *Drug Metab. Dispos.* **1997**, *25*, 805−813.
(10) Romão, M. J.; Archer, M.; Moura, I.; Moura, J. J. G.; LeGall, J.; Engh, R.; Schneider, M.; Hof, P.; Huber, R. *Science* **1995**, *270*, 1170−1176.
(11) Huber, R.; Hof, P.; Duarte, R. O.; Moura, J. J. G.; Moura, I.; Liu, M.-Y.; LeGall, J.; Hille, R.; Archer, M.; Romão, M. J. *Proc. Natl. Acad. Sci. U.S.A.* **1996**, *93*, 8846−8851.
(12) Bray, R. C.; Gutteridge, S.; Stotter, D. A.; Tanner, S. J. *Biochem. J.* **1979**, *177*, 357−360.

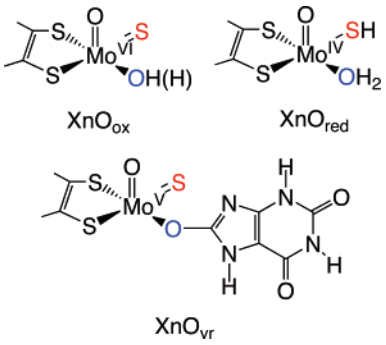

Figure 1. Idealized structures of the oxidized (ox), reduced (red), and very-rapid (vr) forms of xanthine oxidase as derived from crystallographic and spectroscopic studies. The Mo(VI) ion in XnO_{ox} is coordinated by two sulfur donors from the pyranopterin dithiolene, a terminal sulfido, a water/hydroxide, and an apical oxo. The Mo(IV) ion in XnO_{red} is coordinated by two sulfur donors from the pyranopterin dithiolene, a sulfhydryl, a water/hydroxide, and an apical oxo. The very-rapid structure is similar to XnO_{ox} except that the Mo ion is reduced by one electron and the water/hydroxide is replaced by bound product.

debate. Current interpretations of the X-ray crystallographic results for bovine XnO, xanthine dehydrogenase (XnDH) from *Rhodobacter capsulatus*, and the AO from *Desulfovibrio gigas* suggest that their oxidized active sites likely possess a square pyramidal geometry,[10,11,14,15] with the unexpected result that the terminal sulfido ligand occupies the *apical* position. In contrast, more recent crystallographic studies of an XnO catalytic intermediate indicate that the terminal sulfur occupies an equatorial (basal) site.[1] In addition to the sulfido/oxo ligand, a single pyranopterin dithiolene chelate,[16] and a coordinated water/hydroxide[17] directed toward a deep (~15 Å) substrate access channel are believed to complete the equatorial plane.[18−22] A knowledge of the structural and electronic attributes of the $[Mo^{VI}OS]^{2+}$ site is crucial to a full description of the enzyme mechanism.

Probing the active site of XnO directly using optical spectroscopies has proven extremely difficult because of intense absorptions from the Fe_2S_2 and FAD prosthetic groups of the enzyme.[23] Recently, we used freeze−quench difference magnetic circular dichroism (MCD) spectroscopy to trap the paramagnetic "very rapid" intermediate (XnO_{vr}) and probe the excited-state electronic structure of the Mo(V) site under turnover conditions.[24] The XnO_{vr} center has been shown to be a true catalytic intermediate in the turnover of many substrates and is therefore of considerable mechanistic importance.[25,26] The results of this MCD study provided the first evidence for an XnO_{vr} active-site structure where the terminal oxo ligand is oriented cis to both of the dithiolene sulfur donor atoms, effectively placing the oxo ligand in the *apical* position. One of us (M.L.K.) had previously proposed that a geometric change occurs at the Mo site that is induced by substrate binding in the pocket or directly at the active site to be consistent with the X-ray crystallographic interpretations regarding the structure of XnO_{ox}.[24] However, this geometric change is unnecessary if the sulfide-based ligand is located in a basal position as indicated by the most recent protein crystallographic studies.[1] Additionally, the presence of a basal sulfido in XnO_{red} is supported by EPR comparisons between *hpH* and *lpH* sulfite oxidase, and the EPR active "rapid type 1" form of XnO.[27] Finally, the structure of the related bacterial CO dehydrogenase from *Oligotropha carboxidovorans* clearly shows the presence of a basal (bridging) sulfido between the Mo and Cu sites.[28,29]

Valuable insights into the mechanism of XnO have been derived from EPR,[30−38] ESEEM,[39] and ENDOR[25,40−43] spectroscopies of the XnO_{vr} intermediate, believed to contain an $Mo^{V}OS(OR)$ (OR = oxidized substrate) center with a geometry similar to the active site of the oxidized enzyme. Direct evidence for this structure was provided by a ^{13}C ENDOR study of XnO_{vr}, which indicated the presence of an enolate tautomer of bound oxidized product.[25] Furthermore, a series of elegant single turnover ^{17}O labeling experiments[44] showed that the catalytically labile oxygen incorporated into substrate, and bound as ^{17}OR in XnO_{vr}, derives from the metal activated solvent water/hydroxide. This result has significant mechanistic implications regarding how a water derived oxygen atom is incorporated into substrate under turnover conditions. A working mechanistic hypothesis, based upon the ^{13}C ENDOR data, suggests a mechanism of purine hydroxylation that involves base-assisted nucleophilic attack by metal activated hydroxide[17] on the C_8 position of the purine substrate, followed by hydride transfer to the terminal sulfido ligand (Scheme 1).

EPR studies using ^{33}S enriched enzyme have shown that the singly occupied molecular orbital (SOMO, formally the Mo-

(13) D'Ardenne, S. C.; Edmondson, D. E. *Biochemistry* **1990**, *29*, 9046−9052.
(14) Enroth, C.; Eger, B. T.; Okamoto, K.; Nishino, T.; Nishino, T.; Pai, E. F. *Proc. Nat. Acad. Sci. U.S.A.* **2000**, *97*, 10723−10728.
(15) Truglio, J. J.; Theis, K.; Leimkuhler, S.; Rappa, R.; Rajagopalan, V. K.; Kisker, C. V. *Structure* **2002**, *10*, 115−125.
(16) Kirk, M. L.; Helton, M. E.; McNaughton, R. L. *Prog. Inorg. Chem.* **2004**, *52*, 111−212.
(17) Doonan, C. J.; Stockert, A.; Hille, R.; George, G. N. *J. Am. Chem. Soc.* **2005**, *127*, 4518−4522.
(18) Hille, R.; George, G. N.; Eidsness, M. K.; Cramer, S. P. *Inorg. Chem.* **1989**, *28*, 4018−4022.
(19) Cramer, S. P.; Wahl, R.; Rajagopalan, K. V. *J. Am. Chem. Soc.* **1981**, *103*, 7721−7727.
(20) Cramer, S. P.; Hille, R. *J. Am. Chem. Soc.* **1985**, *107*, 8164−8169.
(21) Turner, N. A.; Bray, R. C.; Diakun, G. P. *Biochem. J.* **1989**, *260*, 563−571.
(22) Tullius, T. D.; Kurtz, D. M.; Conradson, S. D.; Hodgson, K. O. *J. Am. Chem. Soc.* **1979**, *101*, 2776−2779.
(23) Komai, H.; Massey, V.; Palmer, G. *J. Biol. Chem.* **1969**, *244*, 1692−1700.
(24) Jones, R. M.; Inscore, F. E.; Hille, R.; Kirk, M. L. *Inorg. Chem.* **1999**, *38*, 4963−4970.
(25) Manikandan, P.; Choi, E.-Y.; Hille, R.; Hoffman, B. M. *J. Am. Chem. Soc.* **2001**, *123*, 2658−2663.
(26) McWhirter, R. B.; Hille, R. *J. Biol. Chem.* **1991**, *266*, 23724−23731.
(27) Peariso, K.; Chohan, B. S.; Carrano, C. J.; Kirk, M. L. *Inorg. Chem.* **2003**, *42*, 6194−6203.
(28) Dobbek, H.; Gremer, L.; Kiefersauer, R.; Huber, R.; Meyer, O. *Proc. Nat. Acad. Sci. U.S.A.* **2002**, *99*, 15971−15976.
(29) Dobbek, H.; Huber, R. In *Metal Ions in Biological Systems. Molybdenum and Tungsten: Their Roles in Biological Processes*; Marcel Dekker: New York, 2002; Vol. 39, pp 227−263.
(30) Bray, R. C.; Vänngård, T. *Biochem. J.* **1969**, *114*, 725−734.
(31) Lowe, D. J.; Barber, M. J.; Pawlik, R. T.; Bray, R. C. *Biochem. J.* **1976**, *155*, 81−85.
(32) George, G. N.; Bray, R. C. *Biochemistry* **1988**, *27*, 3603−3609.
(33) Hawkes, T. R.; Bray, R. C. *Biochem. J.* **1984**, *222*, 587−600.
(34) Malthouse, J. P. G.; Bray, R. C. *Biochem. J.* **1980**, *191*, 265−267.
(35) Malthouse, J. P. G.; Gutteridge, S. S.; Bray, R. C. *Biochem. J.* **1980**, *185*, 767−770.
(36) Malthouse, J. P. G.; George, G. N.; Lowe, D. J.; Bray, R. C. *Biochem. J.* **1981**, *199*, 629−637.
(37) Canne, C.; Lowe, D. J.; Fetzner, S.; Adams, B.; Smith, A. T.; Kappl, R.; Bray, R. C.; Huttermann, J. *Biochemistry* **1999**, *38*, 14077−14087.
(38) Greenwood, R. J.; Wilson, G. L.; Pilbrow, J. R.; Wedd, A. G. *J. Am. Chem. Soc.* **1993**, *115*, 5385−5392.
(39) Lorigan, G. A.; Britt, R. D.; Kim, J. H.; Hille, R. *Biochim. Biophys. Acta* **1994**, *1185*, 284−294.
(40) Howes, B. D.; Pinhal, N. M.; Turner, N. A.; Bray, R. C.; Anger, G.; Ehrenberg, A.; Raynor, J. B.; Lowe, D. J. *Biochemistry* **1990**, *29*, 6120−6127.
(41) Howes, B. D.; Bray, R. C.; Richards, R. L.; Turner, N. A.; Bennett, B.; Lowe, D. J. *Biochemistry* **1996**, *35*, 1432−1443.
(42) Howes, B. D.; Bennett, B.; Bray, R. C.; Richards, R. L.; Lowe, D. J. *J. Am. Chem. Soc.* **1994**, *116*, 11624−11625.
(43) Choi, E. Y.; Stockert, A. L.; Leimkuhler, S.; Hille, R. *J. Inorg. Biochem.* **2004**, *98*, 841−848.
(44) Xia, M.; Dempski, R.; Hille, R. *J. Biol. Chem.* **1999**, *274*, 3323−3330.

Scheme 1. Postulated Mechanism for the Oxidation of Purine Substrates by XnO

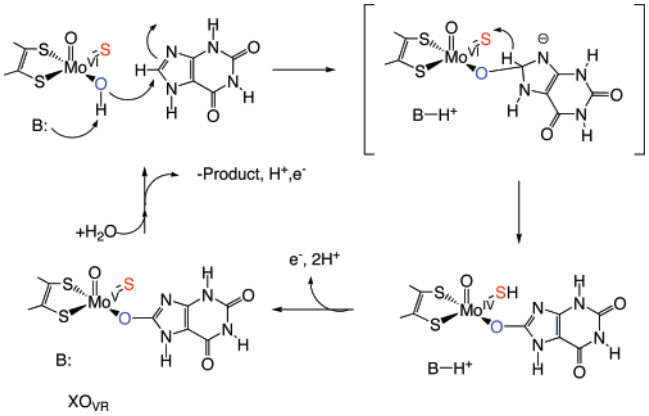

(d_{xy}) orbital) of XnO_{vr} possesses ~38% sulfido character,[32,45] indicating the presence of a strong covalent Mo═S interaction in XnO_{vr} and, by inference, the oxidized $[Mo^{VI}OS]^{2+}$ center in XnO_{ox}. This covalency is likely reduced to a large degree in XnO_{red}, due to protonation of the terminal sulfido. As such, understanding the role of this catalytically essential sulfido ligand[46] in both the oxidative and reductive half reactions of the enzyme is of prime importance in developing a deeper mechanistic insight into XnO and AO mediated catalysis. Ongoing mechanistic debates revolve around the role of the terminal sulfido ligand, as either a proton or hydride acceptor, following hydroxide attack on the purine nucleus.[47−50] Neither of these mechanisms specifically address the influence of the ground-state wave function on reactivity.[51] Here, we utilize small molecule analogues of XnO_{ox} and XnO_{vr}[52,53] to understand the unique intrinsic electronic structure of the $[MoOS]^{2+,1+}$ active site and provide deeper insight into the reactions catalyzed by XnO and AO.

Experimental Methods and Procedures

General. All spectroscopic samples were prepared in an inert atmosphere of N_2 using dried and deoxygenated solvents. The compounds $CoCp_2[Tp^{iPr}Mo^{V}OS(OPh)]$ and $Tp^{iPr}Mo^{VI}OS(OPh)$ (Cp = η^5-cyclopentadienyl; Tp^{iPr} = hydrotris(3-isopropylpyrazol-1-yl)borate) were prepared as previously described.[52,53] Note that the Mo(VI) complex was isolated as a dimer but becomes monomeric in solution).[52,53]

Vibrational Spectroscopy. Raman spectra were collected at room temperature in a 135° backscattering geometry. Coherent Innova (5W) Ar^+ (457.9−528.7 nm, 9 discrete lines) and 300 °C Kr^+ (406.7−676.4 nm, six discrete lines) ion lasers were used as the photon sources. Scattered radiation was dispersed onto a liquid nitrogen cooled 1 in. Spex Spectrum One CCD detector using a Spex 1877E triple grating monochromator equipped with 600, 1200, and 1800 gr/mm holographic gratings at the spectrographic stage. Laser power was measured at the sample and kept below 100 mW to prevent possible photo and thermal degradation of the sample. Solid samples were prepared as finely ground powders and dispersed in a NaCl matrix with $NaNO_3$ added as an internal standard. Solution samples were prepared by dissolving the sample in dichloromethane. These samples were subsequently sealed in an NMR tube and placed into a modified NMR sample holder/spinner for data collection. Infrared spectra were recorded on a Perkin-Elmer 1430 spectrophotometer as pressed KBr disks.

X-ray Absorption Spectroscopy (XAS). X-ray absorption spectroscopic studies were performed at the Stanford Synchrotron Radiation Laboratory with the SPEAR storage ring containing 60−100 mA at 3.0 GeV. Measurements at the molybdenum L- and sulfur K-edge were performed on beamline 6−2 using an Si(111) double crystal monochromator and a wiggler field of 1.0 T. Harmonic rejection was accomplished by using a flat nickel-coated mirror downstream of the monochromator adjusted so as to have a cutoff energy of about 4500 eV. Incident X-ray intensity was monitored using an ion chamber contained in a (flowing) helium-filled flight path. Energy resolution was optimized by decreasing the vertical aperture upstream of the monochromator and quantitatively determined to be 0.51 eV by measuring the width of the 2471.4 eV 1s → $\pi^*(3b_1)$ transition of gaseous SO_2, which corresponds to a one-electron promotion to a single orbital, in contrast to the case for solid standards.[54] X-ray absorption was monitored by recording total electron yield and the energy scale was calibrated with reference to the lowest energy peak of the sodium thiosulfate standard ($Na_2S_2O_3 \cdot 5H_2O$), which was assumed to be 2469.2 eV.[55]

Data were analyzed using the EXAFSPAK suite of computer programs (http://ssrl.slac.stanford.edu/EXAFSPAK.html) and no smoothing or related operations were performed upon the data. Peak positions and the integrated intensities of the features in near-edge spectra were estimated by curve-fitting to a sum of pseudo-Voigt peaks using the program EDG_FIT.[56]

Density Functional Theory Calculations. Density functional theory (DFT) calculations were performed using the Gaussian 03, version B.03 software package.[57] Becke's three-parameter exchange functional[58] combined with Lee, Yang, and Parr's correlation functional[59,60] (B3LYP) were utilized with a 6-31G(d′p′) basis set for all atoms except Mo, where the LANL2DZ basis set and effective core potentials were used. The computational models $(NH_3)_3Mo^{V}OS(OPh)$, $[(NH_3)_3Mo^{VI}OS(OPh)]^+$, $[Mo^{IV}O(SH)(OH_2)(dt)]^-$ and $[Mo^{VI}OS(OH)(dt)]^-$ (dt = *cis*-2-butene-2,3-dithiolate) were employed to minimize computational run times. Here, the arrangement of the three NH_3 donors were used to approximate the coordination environment of the tridentate facial Tp^{iPr} ligand in the synthetic model complexes, and *cis*-2-butene-2,3-dithiolate was used as a model for the ene-1,2-dithiolate portion of the pyranopterin dithiolene cofactor.

The molecular coordinates used in calculations involving the xanthine oxidase active site were based on X-ray crystallographic[14] and extended X-ray absorption fine structure (EXAFS)[22,56,61] data. The orientation of the hydrogen atoms for the coordinated H_2O and OH^- ligands are unknown. As the calculations were relatively insensitive to the position of these protons, initial O_{oxo}−Mo−O−H dihedral angles of 0° were used in both cases. EPR spectroscopy indicates that the sulfhydryl proton is strongly coupled to the ^{95,97}Mo nuclei in XnO rapid type 1 (XnO_{rt1}), and this has been interpreted as resulting from the sulfhydryl proton lying in or near the plane of the d_{xy} redox orbital.[36] Therefore, we have used a 90° O_{oxo}−Mo−S−H initial dihedral angle in the

(45) Wilson, G. L.; Greenwood, R. J.; Pilbrow, J. R.; Spence, J. T.; Wedd, A. G. *J. Am. Chem. Soc.* **1991**, *113*, 6803−6812.
(46) Massey, V.; Edmondson, D. *J. Biol. Chem.* **1970**, *245*, 6595−6598.
(47) Young, C. G.; Wedd, A. G. *J. Chem Soc., Chem. Commun.* **1997**, 1251−1257.
(48) Hille, R. *Chem. Rev.* **1996**, *96*, 2757−2816.
(49) Hille, R. *Biochim. Biophys. Acta* **1994**, *1184*, 143−169.
(50) Hille, R. *J. Biol. Inorg. Chem.* **1996**, *1*, 397−404.
(51) Joshi, H. K.; Enemark, J. H. *J. Am. Chem. Soc.* **2004**, *126*, 11784−11785.
(52) Smith, P. D.; Slizys, D. A.; George, G. N.; Young, C. G. *J. Am. Chem. Soc.* **2000**, *122*, 2946−2947.
(53) Doonan, C. J.; Nielsen, D. J.; Smith, P. D.; White, J. M.; George, G. N.; Young, C. G. *J. Am. Chem. Soc.* **2006**, *128*, 305−316.
(54) Song, I.; Rickett, B.; Janavicius, P.; Payer, J. H.; Antonio, M. R. *Nucl. Instrum. Methods Phys. Res., Sect. A* **1995**, *360*, 634−641.
(55) Sekiyama, H.; Kosugi, N.; Kuroda, H.; Ohta, T. *Bull. Chem. Soc. Jpn.* **1986**, *59*, 575−579.
(56) Pickering, I.; George, G. N. *Inorg. Chem.* **1995**, *34*, 3142−3152.
(57) Frisch, M. J.; et al. *Gaussian 98*, revision A.9; Gaussian, Inc.: Pittsburgh, PA, 1998.
(58) Becke, A. D. *J. Chem. Phys.* **1993**, *98*, 5648−5652.
(59) Miehlich, B.; Savin, A.; Stoll, H.; Preuss, H. *Chem. Phys. Lett.* **1989**, *157*, 200−206.
(60) Lee, C. T.; Yang, W. T.; Parr, R. G. *Phys. Rev. B: Condens. Matter Mater. Phys.* **1988**, *37*, 785−789.
(61) Bordas, J.; Bray, R. C.; Garner, C. D.; Gutteridge, S.; Hasnain, S. S. *Biochem. J.* **1980**, *191*, 499−508.

Scheme 2. 2,6-(1*H*,3*H*,7*H*)-Purinedione Tautomer of Xanthine

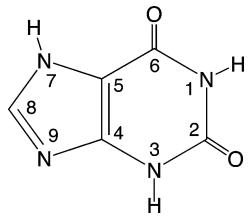

calculations. Molecular coordinates for computational models of $CoCp_2$-[$Tp^{iPr}Mo^{V}OS(OPh)$] and $Tp^{iPr}Mo^{VI}OS(OPh)$ were derived from X-ray crystallographic and EXAFS data.[53]

An additional density functional calculation of the sulfur K near edge spectrum for $Tp^{iPr}Mo^{VI}OS(OPh)$ was performed using the Slater transition state method as implemented in the StoBe software package.[62] The calculation was performed considering all electrons as interacting, within the spin-unrestricted formalism. The DZVP basis set was used for all atoms except the absorber where the extended IGLO-III basis was used.[63] The Becke 88 exchange and Perdew 91 exchange-correlation combination was utilized.[64,65] The calculation provides the energies and intensities of a series of discrete transitions, which in this case are convoluted according to a function that increases with energy. The parameters of the convolution function were fitted to reduce the least-squares variation between the calculated and experimental spectra between 2455 and 2485 eV. The calculated spectrum was shifted by 5.5 eV to account for core hole relaxation effects. The molecular coordinates used in the calculation were based on the reported crystal structure of the related dimer precursor, modified such that the Mo−S distance matches the EXAFS distance reported for the monomer (i.e., 2.15 Å).[52,53]

Xanthine possesses several different tautomeric forms, and recent studies have shown 2,6-(1*H*,3*H*,7*H*)-purinedione (Scheme 2) and 2,6-(1*H*,3*H*,9*H*)-purinedione to be the most stable, the former being stabilized by ∼9 kcal/mol with respect to the latter.[66,67] However, it has been suggested that it is the 2,6-(3*H*,7*H*,9*H*)-purinedione tautomer that is hydroxylated by XnO.[67] The argument here is that an energetically destabilized tautomer will require less energy to reach the transition state than other more stable forms. Therefore, DFT calculations were performed on various xanthine tautomers to assess their frontier orbital nature.

Results and Analysis

X-ray Absorption Spectroscopy. Near-Edge Spectra. The normalized sulfur K-edge X-ray absorption near-edge spectroscopy (XANES) spectrum of $Tp^{iPr}Mo^{VI}OS(OPh)$ is displayed in Figure 2 (inset). Three intense preedge features are observed at 2465.9, 2467.1, and 2469.1 eV. These transitions arise from S(1s)→ S(3p) + Mo(4d) transitions and provide a sensitive probe of the degree of S p-orbital character covalently mixed into the Mo d-orbitals (vide infra). The background subtracted preedge region of the sulfur K-edge XANES spectrum (2450−2473 eV) clearly shows the individual transitions that contribute to the S K-preedge region of the spectrum (Figure 2). Inspection of the data reveals that the three observed S(1s) → S(3p) + Mo(4d) transitions possess different intensities and corresponding oscillator strengths. This is indicative of anisotropic sulfur covalency contributions to the Mo−$S_{sulfido}$ bonding scheme (vide infra).

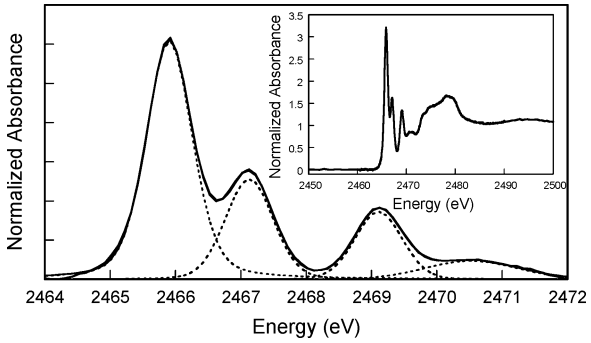

Figure 2. Resolved preedge region of $Tp^{iPr}Mo^{VI}OS(OPh)$ XAS spectrum. The inset shows the normalized sulfur K-edge XANES spectrum of Tp^{iPr}-$Mo^{VI}OS(OPh)$.

Molybdenum L-edges probe the metal d character in the frontier molecular orbital manifold through symmetry allowed transitions between p and d type orbitals. Furthermore, the sharp line widths of Mo L-edges can facilitate resolution of the d-orbital splitting pattern. Figure S1 displays the molybdenum L_2 edge spectrum of $Tp^{iPr}MoOS(OPh)$ and its third derivative. The Mo(2p) → Mo($4d_{xy}$) transition is observed as an inflection point at 2626.6 eV, situated ∼1 eV in energy below the more intense Mo(2p) → Mo($4d_{xz,yz}$) transition, which is rendered spectroscopically degenerate as a consequence of strong π interactions with the terminal oxo ligand.[16,68−70] Importantly, this energy separation is fully consistent with the observation of an ∼8000 cm^{-1} $\psi_{xy} \rightarrow \psi_{xz,yz}$ (ψ_M = the Mo(4d) molecular orbitals; $\chi_{S(3p)}$ (and similar notation) = S(3p) atomic orbitals in the LCAO expansion of the formally Mo(4d) molecular orbitals (ψ_M); $\varphi_{Mo(4d)}$ = Mo(4d) atomic orbitals in the LCAO expansion of the formally Mo(4d) molecular orbitals (ψ_M)) ligand-field band in the electronic absorption spectrum of $CoCp_2$[Tp^{iPr}-MoOS(OPh)] (Figure S2).[71] The Mo(2p) → Mo($4d_{xz,yz}$), Mo(2p) → Mo($4d_{x^2-y^2}$), and Mo(2p) → Mo($4d_{z^2}$) transitions are clearly visible at 2627.6, 2629.7, and 2630.7 eV, respectively. The relatively low energy of the Mo(2p) → Mo($4d_{z^2}$) transition leads to a 4.1 eV spectroscopic splitting of the Mo($4d_{xy}$) and Mo($4d_{z^2}$) orbitals, and this is likely a function of the strong Mo($4d_{xy}$)−S(3p) bonding interaction which increases the energy of the Mo($4d_{xy}$) orbital by approximately 1 eV through π interactions with the terminal sulfido ligand (vide infra).

Evaluation of Mo−$S_{sulfido}$ Covalency. X-ray absorption spectroscopy at the S K-edge is one of the most direct and powerful spectroscopic probes of sulfur covalency contributions to the overall metal−ligand bonding scheme.[72] This is a result of the fact that transitions in the preedge region are bound state transitions that arise from dipole allowed S(1s) core one-electron promotions to valence molecular orbitals with S(3p) character. Since the S(3p) orbitals are completely occupied, the observed

(62) Triguero, L.; Pettersson, L. G. M. G. M.; Agren, H. *Phys. Rev. B: Condens. Matter Mater. Phys.* **1998**, *58*, 8097−8110.
(63) Kutzelnigg, W.; Fleischer, U.; Schindler, M., *NMR Basic Principles and Progress*; Springer-Verlag: Heidelberg, Germany, 1990; Vol. 23, p 165.
(64) Perdew, J. P. P.; Wang, Y. *Phys. Rev. B: Condens. Matter Mater. Phys.* **1992**, *45*, 13244−13249.
(65) Becke, A. D. *J. Chem. Phys.* **1988**, *88*, 2547−2553.
(66) Kim, J. H.; Odutola, J. A.; Popham, J.; Jones, L.; von Laven, S. *J. Inorg. Biochem.* **2001**, *84*, 145−150.
(67) Ilich, P.; Hille, R. *Inorg. Chim. Acta* **1997**, *263*, 87−93.
(68) Inscore, F. E.; McNaughton, R.; Westcott, B. L.; Helton, M. E.; Jones, R.; Dhawan, I. K.; Enemark, J. H.; Kirk, M. L. *Inorg. Chem.* **1999**, *38*, 1401−1410.
(69) McNaughton, R. L.; Rubie, N. D.; Helton, M. E.; Kirk, M. L. *Abstr. Pap. Am. Chem. Soc.* **1999**, *217*, U1085.
(70) McNaughton, R. L.; Helton, M. E.; Cosper, M. M.; Enemark, J. H.; Kirk, M. L. *Inorg. Chem.* **2004**, *43*, 1625−1637.
(71) Rubie, N. D.; Doonan, C. J.; Young, C. G.; Kirk, M. L. Manuscript in preparation.
(72) Solomon, E. I.; Randall, D. W.; Glaser, T. *Coord. Chem. Rev.* **2000**, *200*, 595−632.

transitions are formally S(1s) → S(3p) + Mo(4d) and the transition intensities are directly proportional to the square of the S(3p) atomic orbital coefficient (α) in the LCAO expansion of the formally Mo(4d) orbitals (ψ_M) according to

$$\psi_M = \sqrt{1-\alpha^2}\,\varphi_{\mathrm{Mo(4d)}} - \alpha\chi_{\mathrm{S(3p)}} \qquad (1)$$

The best fits to the near-edge region were found to require equal contributions of Gaussian and Lorentzian functions in the pseudo-Voigt fits to both the absorption data and its second derivative. The best fits produced residuals of <1.5% in both cases. The integrated intensities of the 2465.9, 2467.1, and 2469.1 eV features were determined to be 2.5 (fwhm = 0.4 eV), 1.2 (fwhm = 0.45 eV), and 1.1 (fwhm = 0.55 eV), respectively. The peak widths are consistent with each feature corresponding to a single transition, as calibrated by Shadle et al.[73] using a series of Cu(II) model complexes. A fourth, weak feature is observed at ~2470 eV, and was included in the fit to properly model the high-energy region of the preedge. However, because of the breadth of the feature (fwhm ≈ 0.9 eV) and its proximity to the S edge, it is very difficult to separate the individual electronic transitions and/or potential continuum resonances that contribute to this feature. Normalization of the integrated intensities for the three lowest energy preedge features yields an intensity ratio of 1.00:0.48:0.44 demonstrating that, while there is significant sulfur character mixed into the higher energy Mo d orbitals, the S character is clearly greatest in the ψ_{xy} π^* lowest unoccupied molecular orbital (LUMO), viz., the redox active molecular orbital.

Owing to the lack of a covalency calibration for Mo-sulfido complexes, we are only able to determine the relative S contributions to ψ_{xy}, $\psi_{xz,yz}$, and $\psi_{x^2-y^2}$ from these spectra. Note that S contributions to ψ_{z^2} are not observed owing to the high energy of this d orbital (σ^* with the apical oxo) and the fact that the S donor is precluded from appreciable interactions with ψ_{z^2} as a result of the poor overlap imposed by the cis oxo-sulfido geometry in the complex. However, ^{33}S EPR studies on the XnO_{vr} intermediate have shown that there is ~38% $S_{sulfido}$ character in ψ_{xy},[32,45] which is in good agreement with the ~30 to 41% $S_{sulfido}$ character determined by DFT for $[(NH_3)_3Mo^{VI}OS(OR)]^+$. The orbital covalency parameters derived from DFT calculations on $[(NH_3)_3Mo^{VI}OS(OMe)]^+$ show the $S_{sulfido}$ contributions to the ψ_{xy}, $\psi_{xz,yz}$, and $\psi_{x^2-y^2}$ acceptor orbitals to be 41%, 18%, and 17%, respectively, while those determined for $[(NH_3)_3Mo^{VI}OS(OPh)]^+$ yield $S_{sulfido}$ contributions to the ψ_{xy}, $\psi_{xz,yz}$, and $\psi_{x^2-y^2}$ acceptor orbitals of 30%, 25%, and 16%, respectively. The relative Mo−S covalency ratios determined from the DFT calculation on $[(NH_3)_3Mo^{VI}OS(OMe)]^+$ are 1.00:0.44:0.41, whereas that for $[(NH_3)_3Mo^{VI}OS(OPh)]^+$ is 1.00:0.83:0.53. The calculated covalency ratios for $[(NH_3)_3Mo^{VI}OS(OMe)]^+$ and $[(NH_3)_3Mo^{VI}OS(OPh)]^+$ are in remarkable agreement with those determined experimentally (1.00:0.48:0.44) from the S near-edge spectrum (Figure 2). In summary, the results of the DFT calculations, as well as the large Mo−$S_{sulfido}$ covalency indicated by the S K-edge XAS data, imply significant Mo−$S_{sulfido}$ multiple bond character in ψ_{xy}.

We have also performed DFT calculations using the Slater transition-state method to explicitly evaluate the oscillator strengths of the individual transitions that comprise the near edge region of $Tp^{iPr}Mo^{VI}OS(OPh)$ using the computational model TpMoOS(OPh) (Tp = hydrotris(pyrazol-1-yl)borate). Additionally, these calculations allow for a direct comparison of covalency contributions to the Mo−S bonding scheme determined by this method with the aforementioned ground-state calculations. The theoretical spectrum generated from the Slater transition-state method and selected acceptor orbitals are given in Figure 3. The acceptor orbital for the lowest energy transition is the LUMO (ψ_{xy}), which is Mo(d_{xy})-S^{π} antibonding in character and contains significant contributions from φ_{xy}, $\chi_{S^{\pi}}$, and $\chi_{O^{\sigma}}$ atomic orbitals (Figure 4). The LUMO+1 (ψ_{xz}) contains contributions from φ_{xz} and $\chi_{S^{\nu}}$, while the LUMO+2 orbital (ψ_{yz}) is comprised mostly of φ_{yz} with some $\chi_{O^{\nu}}$ character deriving from the phenolate ligand. The fourth acceptor orbital (LUMO+3; isosurface not shown in Figure 3) possesses pyrazole π^* character based on the pyrazole ring oriented trans to the sulfido. We have observed that the π-acceptor character of the Tp ligand in DFT calculations is often overemphasized, that is, the pyrazolyl π^* orbitals are too low in energy. Currently, there is no spectroscopic evidence that Tp, Tp* (Tp* = hydrotris(3,5-dimethylpyrazol-1-yl)borate) and related ligands participate as π acceptor ligands in d^1 Mo(V) metal-to-ligand charge transfer (MLCT) transitions. The $\varphi_{x^2-y^2}$ atomic orbital (LUMO+4) is σ-antibonding in nature and mixes with the sulfido $\chi_{S^{\sigma}}$ and phenolate $\chi_{O^{\nu}}$ and $\chi_{O^{\sigma}}$ ligand orbitals in addition to the

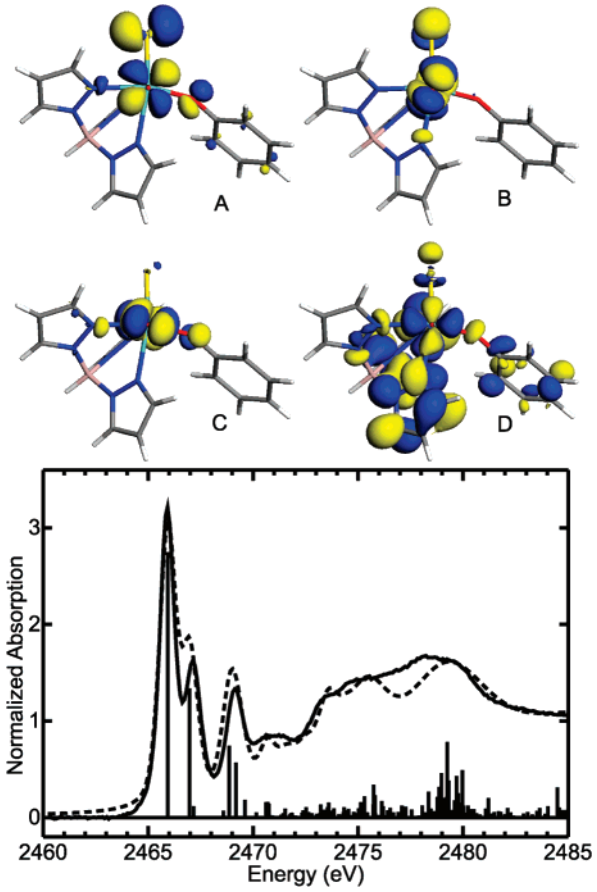

Figure 3. Results of Slater transition-state calculations. Top: Four of the lowest energy acceptor orbitals for the $TpMo^{VI}OS(OPh)$ computational model (0.05 au isosurface plots): (A) LUMO; (B) LUMO+1; (C) LUMO+2; (D) LUMO+4. Bottom: Theoretical spectrum (dashed), compared with the experimental S K-edge spectrum (solid) of $Tp^{iPr}Mo^{VI}OS(OPh)$.

(73) Shadle, S. E.; Pennerhahn, J. E.; Schugar, H. J.; Hedman, B.; Hodgson, K. O.; Solomon, E. I. *J. Am. Chem. Soc.* **1993**, *115*, 767−776.

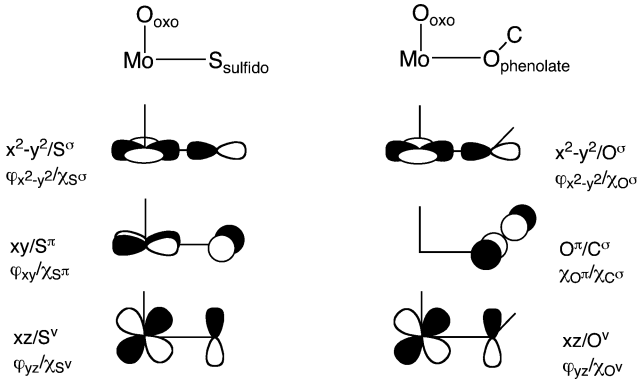

Figure 4. Idealized sulfido (S) and phenolate (O) interactions with the molybdenum d orbitals: (right) the $O_{oxo}-Mo-O_{phenolate}-C$ dihedral angle is 90°.

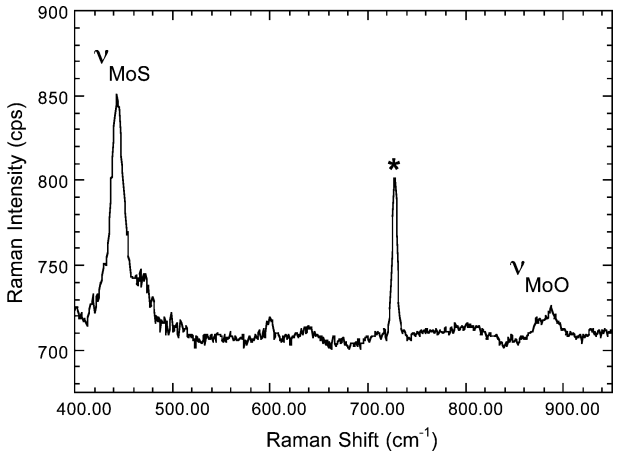

Figure 5. Room-temperature Raman spectrum at 457.9 nm of solid $CoCp_2[Tp^{iPr}Mo^{V}OS(OPh)]$ dispersed in $NaCl/NaNO_3$. Nitrate band is marked with an asterisk.

π^* orbitals of both the phenolate and pyrazole rings. This results in a highly delocalized molecular orbital with $\varphi_{x^2-y^2}$ character being present in both the LUMO+4 and LUMO+5. Finally, the S p-orbital character present in ψ_{xy} for the Slater transition-state calculation is only ~24%. This is markedly lower than the calculated sulfido covalency contribution to ψ_{xy} from the ground-state calculations using either Gaussian (30−41%), StoBe (32%), or Dmol (37%). This apparent discrepancy is due to the presence of half a core hole on the sulfido in the transition-state calculation, which lowers the energy of the sulfido p orbitals to a much greater extent than the corresponding Mo d orbitals. The net effect is a reduction in Mo−S mixing and a corresponding reduction in Mo-S covalency. The same effect, resulting from the presence of half a core hole on the sulfido in the transition state, is also observed for the other acceptor orbitals, with a corresponding decrease in Mo−S covalency. Regardless of these covalency differences, the ratio of the calculated oscillator strengths to the degree of sulfido p-orbital character covalently mixed into ψ_{xy}, $\psi_{xz,yz}$, and $\psi_{x^2-y^2}$ (1.0:0.48:0.45) is virtually the same as that derived from the ground-state calculations.

Raman Spectroscopy. Spectral Data. The Raman spectrum of solid $CoCp_2[Tp^{iPr}Mo^{V}OS(OPh)]$ dispersed in an $NaCl/NaNO_3$ matrix is shown in Figure 5. Raman spectra for $CoCp_2[Tp^{iPr}Mo^{V}OS(OPh)]$ were only obtained in the solid state, since solution samples suffered from photo and/or thermal degradation even when laser powers were maintained at or below ~60 mW. The Mo(VI) compound $Tp^{iPr}Mo^{VI}OS(OPh)$ can only be generated upon solvation, which results in the cleavage of the disulfide bond of the dimeric precursor. Therefore, we are limited to Raman studies of $Tp^{iPr}Mo^{VI}OS(OPh)$ in solution. The Raman spectra of $CoCp_2[Tp^{iPr}Mo^{V}OS(OPh)]$ and $Tp^{iPr}Mo^{VI}OS(OPh)$ reveal Mo−O_{oxo} (ν_{MoO}) vibrational frequencies of 888 cm^{-1} (890 cm^{-1} IR) and 912 cm^{-1} (917 cm^{-1} IR), respectively, and Mo−S (ν_{MoS}) frequencies of 444 cm^{-1} (440 cm^{-1} IR) and 486 cm^{-1} (483 cm^{-1} IR), respectively.[53] The Mo−O_{oxo} vibrational frequency falls within the range of ν_{MoO} values reported for other oxomolybdenum compounds (~850 to 1050 cm^{-1}).[74,75] However, ν_{MoS} is notably less than 525 cm^{-1}, the $\nu_{Mo\equiv S}$ stretching frequency reported for the formally triply-bonded terminal sulfido compound Tp^*MoSCl_2.[75] The results are consistent with a significant reduction in bond order for the Mo−S bond in the [MoOS] unit compared with the formal triple Mo≡S bond present in terminal metal-sulfido complexes devoid of oxo ligation.

Valence Bond Description of the Mo−S Bond Order. The Mo−S and Mo−O_{oxo} stretching modes occur at relatively high frequency and, in principle, allow for an assessment of the Mo−S bond order in these small molecule analogues and, by inference, enzymes of the XnO family. As previously noted, the vibrational Raman results show that the Mo−O_{oxo} stretching frequency is in the range observed for Mo≡O frequencies in monooxomolybdenum compounds (~850 to 1050 cm^{-1}).[74,75] Thus, a Mo−S bond oriented cis to Mo−O_{oxo} does not appear to appreciably affect the nature of Mo−O_{oxo} bonding in $[Tp^{iPr}MoOS(OPh)]^{0,1-}$, and the Mo−$O_{oxo}$ bond likely retains its formal triple-bond character with the O_{oxo} p_z orbital (χ_{O^z}) interacting in a σ sense with φ_{z^2}, and χ_{O^x} and χ_{O^y} forming π bonds with $\varphi_{xz,yz}$. A formal triple bond is also possible for the Mo−S bond in the [MoOS] unit. Therefore, fundamental questions arise regarding the nature of the Mo−S bond order in [MoOS] centers and how the Mo d orbitals are partitioned to take part in the [MoOS] bonding scheme.

As the value for ν_{MoS} observed in Tp^*MoSCl_2 is significantly higher than the 486 and 444 cm^{-1} modes observed for Tp^{iPr}-$MoOS(OPh)$ and $CoCp_2[Tp^{iPr}MoOS(OPh)]$, respectively, a reduction in Mo−S bond order is suggested for the latter two compounds. Presumably, the frequency reduction is more dramatic in $CoCp_2[Tp^{iPr}Mo^{V}OS(OPh)]$ because an electron now occupies the ψ_{xy} Mo−S π^* orbital, therefore weakening the bond and lowering the observed vibrational frequency. At this point, we make the approximation that the Mo−O_{oxo} and Mo−S vibrations are *uncoupled*, the principal components of these vibrations are heteronuclear diatomic in nature, and the bond order is proportional to the harmonic force constants derived from vibrational spectroscopy. It must be stated that the relationship between force constant and bond order is more complicated than these initial assumptions suggest. Namely, the bond order is proportional to the depth of the anharmonic potential well and the force constants are proportional to the curvature of the potential well. However, to the extent that an empirical relationship exists between force constant and bond order, vibrational spectroscopy can be used to help assess the nature of the bonding. As such, we describe these high-frequency modes within a harmonic oscillator approximation,

(74) Johnson, M. K. *Prog. Inorg. Chem.* **2004**, *52*, 213−266.
(75) Backes, G.; Enemark, J. H.; Loehr, T. M. *Inorg. Chem.* **1991**, *30*, 1839−1842.

where the following equations are relevant to the further analysis of the vibrational data.[76]

$$\tilde{\nu}\ (\mathrm{cm}^{-1}) = \frac{\nu}{c} = 1303.1\sqrt{\frac{K_{\mathrm{MoS}}}{\mu}} \qquad (2)$$

Here $\tilde{\nu}$ is the Mo−S vibrational frequency (ν_{MoS}) in wavenumbers, $\mu = 24.03$ g·mol^{-1} is the reduced mass, K is the harmonic oscillator force constant in mdyne/Å, and the other symbols have their usual meanings.

To first order, Tp*Mo^{V}SCl$_2$ is assumed to possess a Mo≡S triple bond, in analogy with the Mo−O$_{oxo}$ bonding scheme in the related compound, Tp*Mo^{V}OCl$_2$.[77] Because the triple bond is formed from S 3p orbital interactions with Mo φ_{z^2} (σ) and $\varphi_{xz,yz}$ (π) orbitals, an unpaired electron in the ψ_{xy} orbital does not affect the formal Mo−S bond order. This results from the fact that the ψ_{xy} orbital in Tp*Mo^{V}SCl$_2$ is orthogonal to the Mo−S bond and does not participate in the Mo≡S bonding scheme. As the XAS data and DFT calculations support a strong Mo−S d−p π* interaction in Tp$^{i\mathrm{Pr}}$Mo^{VI}OS(OPh), a high Mo−S bond order is also anticipated.

If it is assumed that the terminal oxo donor in Tp$^{i\mathrm{Pr}}$Mo^{VI}OS(OPh) and CoCp$_2$ [Tp$^{i\mathrm{Pr}}$Mo^{V}OS(OPh)] dominates the ligand field and is triply bonded to the metal, valence bond theory indicates that only the Mo ψ_{xy} and $\psi_{x^2-y^2}$ orbitals are left for significant σ and π bonding interactions with the sulfido ligand. Therefore, the Mo−S bond orders for $[MoOS]^{2+}$ and $[MoOS]^{+}$ complexes are anticipated to be 2 ($\sigma + \pi$) and 1.5 ($\sigma + 0.5\pi$), respectively. The determination of harmonic oscillator force constants for the Mo−S bond in Tp*Mo^{V}SCl$_2$, Tp$^{i\mathrm{Pr}}$Mo^{VI}OS(OPh), and CoCp$_2$[Tp$^{i\mathrm{Pr}}$Mo^{V}OS(OPh)] provide for an internal check of the formal Mo−S bond orders predicted for these three complexes. We start by partitioning K_{MoS} for Tp*Mo^{V}SCl$_2$, which possesses a formal triple bond, into its σ and π components according to $K_{\mathrm{MoS}} = K_\sigma + 2K_\pi$. Similarly, for CoCp$_2$[Tp$^{i\mathrm{Pr}}$Mo^{V}OS(OPh)] the Mo−S force constant $K'_{\mathrm{MoS}} = K_\sigma + 0.5K_\pi$. Substitution of the observed Mo−S vibrational frequencies, ν_{MoS}, for CoCp$_2$[Tp$^{i\mathrm{Pr}}$Mo^{V}OS(OPh)] and Tp*Mo^{V}SCl$_2$ into eq 2 and solving the two simultaneous equations yields $K_\sigma = 2.42$ mdyne/Å and $K_\pi = 0.74$ mdyne/Å. Provided that our approximations yield reasonable partitioned harmonic oscillator force constants, K_σ and K_π, they should accurately reproduce the Mo−S vibrational frequency for Tp$^{i\mathrm{Pr}}$Mo^{VI}OS(OPh). However, as there is an oxidation state change between CoCp$_2$[Tp$^{i\mathrm{Pr}}$Mo^{V}OS(OPh)] and Tp$^{i\mathrm{Pr}}$Mo^{VI}OS(OPh), we will use their respective ν_{MoO} frequencies to assess the effects of oxidation state on the force constant using the following ratio:

$$\frac{\tilde{\nu}_{\mathrm{Mo^{V}O}}}{\tilde{\nu}_{\mathrm{Mo^{VI}O}}} \propto \sqrt{\frac{K_{\mathrm{Mo^{V}O}}}{K_{\mathrm{Mo^{VI}O}}}} \qquad (3)$$

This analysis shows K_{MoO} increases by 5% upon oxidation of CoCp$_2$[Tp$^{i\mathrm{Pr}}$Mo^{V}OS(OPh)] to Tp$^{i\mathrm{Pr}}$Mo^{VI}OS(OPh). The increase in K_{MoO} results from a corresponding increase in the effective nuclear charge (Z_{eff}) at the Mo center that accompanies the one electron oxidation. Assuming that K_{MoS} also increases by 5% upon oxidation, the partitioned K_σ and K_π are increased to $K_\sigma = 2.55$ and $K_\pi = 0.78$ mdyne/Å for Tp$^{i\mathrm{Pr}}$Mo^{VI}OS(OPh). Using these partitioned force constants, ν_{MoS} for Tp$^{i\mathrm{Pr}}$Mo^{VI}OS(OPh) was determined to be 485 cm^{-1}, which compares exceptionally well with the experimentally determined ν_{MoS} Raman frequency of 486 cm^{-1}. The ability to treat the ν_{MoO} and ν_{MoS} vibrations as primarily heterodiatomic in nature is supported by the DFT calculations, which show an essentially pure Mo−O component to ν_{MoO} and a relative weight of MoS/MoN$_{\mathrm{trans}} \approx 11$ for ν_{MoS}. In summary, a harmonic oscillator approximation may be used for these high-frequency modes to determine partitioned force constants, K_σ and K_π, which in turn may be used to show that the bonding in the *cis*-[MoOS] unit is best described as possessing *dual two-center bonding schemes* with a triply bonded Mo≡O and doubly bonded Mo═S.

Insight into the nature of the Mo−S$_{\mathrm{sulfido}}$ bond can now be evaluated by combining the results of the XAS and vibrational experiments. The S K-edge XAS experiment only determines the Mo(d)−S(p) contribution to the bond covalency, while the magnitude of the force constant reflects ionic and covalent contributions, including Mo(p)−S(p) covalent contributions, to the Mo═S bond. The XAS data clearly indicate that Mo(d)−S(p) π covalency dominates over Mo(d)−S(p) σ bond covalency by a factor of 2−3. Conversely, the experimentally determined partitioned force constants indicate that the σ bond is approximately three times stronger than the π bond. These apparently conflicting data can be easily rationalized if the dominant contributions to the Mo═S bond strength derive from ionic and/or Mo(p)−S(p) covalent bonding interactions and not Mo(d)−S(p) π or Mo(d)−S(p) σ bond covalency. Thus, electron occupancy of ψ_{xy} may activate the Mo═S bond by changing the relative electro-/nucleophilicity of the terminal sulfido (vide infra).

The ability to treat the ν_{MoS} and ν_{MoO} vibrational modes as uncoupled harmonic oscillators is also advantageous with respect to calculating predicted Mo≡O and Mo═S bond lengths in structurally uncharacterized [MoOS] sites. The relationship between the force constant (K) and the internuclear distance for several homo- and heteronuclear diatomic molecules has been studied extensively and is shown to behave in a predictable manner.[78−80] These parameters are related by Badger's Rule,[78,79] shown in eq 4,

$$r_{\mathrm{e}} = \left(\frac{C_{ij}}{10K_{\mathrm{e}}}\right)^{1/3} + d_{ij} \qquad (4)$$

where r_{e} is the internuclear distance (bond length) in Ångstrom units, K_{e} is the force constant in units of mdynes/cm, and C_{ij} and d_{ij} are dependent on the atoms that compose the diatomic species in question. The values of C_{ij} and d_{ij} are determined by the row of the periodic table in which the elements are found and have been tabulated.[79] The appropriate Badger's Rule constants for Mo and S have been used to calculate the Mo−S bond lengths using the unpartitioned force constants for CoCp$_2$[Tp$^{i\mathrm{Pr}}$Mo^{V}OS(OPh)] and Tp$^{i\mathrm{Pr}}$Mo^{VI}OS(OPh) that were derived from their respective ν_{MoS} vibrational frequencies. The calculated Mo−S and Mo−O$_{oxo}$ bond lengths for Tp$^{i\mathrm{Pr}}$Mo^{VI}OS(OPh) are 2.2 and 1.7 Å, respectively. These compare nicely with the

(76) Czernuszewicz, R. S.; Spiro, T. G. In *Inorganic Electronic Structure and Spectroscopy*; Solomon, E. I., Lever, A. B. P., Ed.; John Wiley and Sons, Inc.: New York, 1999; Vol. I, pp 353−442.
(77) Young, C. G.; Enemark, J. H.; Collison, D.; Mabbs, F. E. *Inorg. Chem.* **1987**, *26*, 2925−2927.
(78) Badger, R. M. *J. Chem. Phys.* **1934**, *2*, 128−131.
(79) Badger, R. M. *J. Chem. Phys.* **1935**, *3*, 710.
(80) Gordy, W. *J. Chem. Phys.* **1946**, *14*, 305−313.

experimental Mo−S (2.132(2) Å) and Mo−O_{oxo} (1.692(1) Å) bond lengths determined by molybdenum K-edge EXAFS and the X-ray structure of $Tp^{iPr}MoOS(OC_6H_4{}^sBu\text{-}2)$.[52,53] Thus, an experimental determination of the key ν_{MoS} and ν_{MoO} vibrational modes in various XnO and AO enzyme forms could be used to assess various perturbations on the active site structure due to pH, substrate binding, association with bound product, etc. Of particular importance is the observation of a hydrogen-bonding interaction between Q197 and the apical oxo in *R. capsulatus* xanthine dehydrogenase (XDH), a member of the XnO family. Recently, resonance Raman spectra were collected for XnO_{ox}, using laser excitation between 400 and 650 nm.[81] The ν_{MoO} vibrational mode was observed at 899 cm^{-1} and ν_{MoS} at 474 cm^{-1}; the latter shifted to 462 cm^{-1} upon ^{34}S isotopic substitution.[81] These stretching frequencies compare well with 912 cm^{-1} for ν_{MoO} and 486 cm^{-1} for ν_{MoS} in $Tp^{iPr}Mo^{VI}OS(OPh)$. A Badger's Rule analysis[78,79] with the experimentally determined K_{MoO} and K_{MoS} force constants determined for $Tp^{iPr}Mo^{VI}OS(OPh)$ indicates that the Mo≡O_{oxo} and M═$S_{sulfido}$ bonds are slightly longer in XnO_{ox} relative to the model. Site-directed mutagenesis studies of *R. capsulatus* XDH indicate that the Q197E mutant possesses a 6-fold reduction in k_{red}, and the retarded rate in the mutant has been interpreted as resulting from a change in hydrogen-bonding interactions with the apical oxo.[82] Although our analysis of the vibrational spectra are also consistent with weak hydrogen-bonding interactions between the terminal oxo and the protein, and a slightly longer Mo≡O bond, additional studies are warranted to fully address this issue.

Model, Active Site, and Substrate Bonding Calculations. Bonding calculations were performed at the DFT level of theory on XnO_{ox}, XnO_{red}, the XnO_{ox} models, $[(NH_3)_3Mo^{VI}OS(OR)]^+$ (R = Me. Ph), and the native substrate, xanthine, to gain insight into possible orbital interactions between this substrate and the XnO_{ox} active site. Importantly, the bonding calculations for the XnO_{ox} models $[(NH_3)_3Mo^{VI}OS(OMe)]^+$ and $[(NH_3)_3Mo^{VI}OS(OPh)]^+$ are in excellent agreement with the computational results for XnO_{ox} and indicate a highly covalent LUMO that is composed of ∼35% S(p) and ∼50% Mo(d_{xy}) orbital character. Furthermore, the calculated sulfido character in the XnO_{ox} Mo(d_{xy}) molecular orbital is in remarkable agreement with the spin density distribution determined for the Mo−$S_{sulfido}$ d_{xy}−p_π orbital in XnO_{vr} using ^{33}S EPR spectroscopy, providing an excellent calibration point for quantitating Mo−S covalency determined by S K-preedge XAS.

Table 1 provides a detailed listing of the atomic orbital character for relevant molecular orbitals of $[(NH_3)_3Mo^{VI}OS(OMe)]^+$, $[(NH_3)_3Mo^{VI}OS(OPh)]^+$, $[Mo^{VI}OS(OH)(dt)]^-$, and $[Mo^{IV}O(SH)(OH_2)(dt)]^-$, computational models for $Tp^{iPr}Mo^{VI}OS(OPh)$, XnO_{ox}, and XnO_{red}, respectively. The two electron reduction of $[Mo^{VI}OS(OH)(dt)]^-$ to yield $[Mo^{IV}O(SH)(OH_2)(dt)]^-$ is observed to result in a large reduction in Mo−$S_{sulfido/sulfhydryl}$ bond covalency. This is consistent with the presence of the sulfhydryl donor in $[Mo^{IV}O(SH)(OH_2)(dt)]^-$. Inspection of the atomic orbital character for $[Mo^{IV}O(SH)(OH_2)(dt)]^-$ shows that the sulfhydryl donor contributes only ∼3% of the atomic orbital character to the highest occupied molecular orbital (HOMO); an ∼90% decrease, compared to $[Mo^{VI}OS(OH)(dt)]^-$, in the total terminal $S_{sulfido/sulfhydryl}$ donor character contributing to this MO. A key observation here is that the *decrease* in Mo−$S_{sulfido/sulfhydryl}$ sulfur character that accompanies reduction results in a substantial (∼200%) *increase* in the dithiolene character present in the XnO_{red} Mo(d_{xy}) HOMO.

Table 1

$[(NH_3)_3Mo^{VI}OS(OMe)]^+$ Orbital Composition

MO	Mo %	$S_{sulfido}$%	O (OMe) %	O_{oxo} %
d_{z^2}	48	6	1	10
$d_{x^2-y^2}$	55	17	7	3
d_{yz}	60	9	4	21
d_{xz}	60	9	3	21
d_{xy}	51	41	5	0
sum %	274	82	20	55

$[(NH_3)_3Mo^{VI}OS(OPh)]^+$ Orbital Composition

MO	Mo %	$S_{sulfido}$%	O (OPh) %	O_{oxo}%
d_{z^2}	52	4	3	17
$d_{x^2-y^2}$	57	16	6	3
d_{yz}	59	11	3	20
d_{xz}	59	14	4	18
d_{xy}	54	30	4	2
sum %	281	75	20	60

$[Mo^{VI}OS(OH)(dt)]^-$ (O≡Mo−O−H Dihedral Angle = 0°) Orbital Composition

MO	Mo %	$S_{sulfido}$ %	O_{oxo} %	O(H) %	$S_{dithiolene}$ %
d_{z^2}	66	3	13	4	11
$d_{x^2-y^2}$	54	18	6	2	13
d_{yz}	54	14	16	0	14
d_{xz}	63	1	22	1	9
d_{xy}	54	31	1	8	5
sum %	291	67	58	15	52

$[Mo^{VI}OS(OH)(dt)]^-$ (O≡Mo−O−H Dihedral Angle = 94°) Orbital Composition

MO	Mo %	$S_{sulfhydryl}$ %	O_{oxo} %	O(H) %	$S_{dithiolene}$ %
d_{z^2}	66	4	17	4	7
$d_{x^2-y^2}$	55	15	2	3	15
d_{yz}	55	13	16	1	14
d_{xz}	63	0	20	2	11
d_{xy}	54	32	1	8	5
sum %	293	64	56	18	52

$[Mo^{IV}O(SH)(OH_2)(dt)]^-$ Orbital Composition

MO	Mo %	$S_{sulfhydryl}$ %	O_{oxo} %	$O(H_2)$ %	$S_{dithiolene}$ %
d_{z^2}	70	3	9	0	13
$d_{x^2-y^2}$	65	8	16	0	8
d_{yz}	63	2	8	1	3
d_{xz}	74	1	9	1	3
d_{xy}	67	3	2	0	16
sum %	339	17	44	2	43

For orbitally controlled reactions, electronic structure descriptions of the active site LUMO *and* the substrate HOMO are desirable to understand potential orbital pathways for electron flow from the electron reservoir (substrate) to the electron sink (Mo(d_{xy})−$S_{sulfido}$(p) π^*). This process should be facilitated by maximal orbital overlap between substrate HOMO and active site LUMO. The key frontier orbitals of the neutral xanthine tautomers are primarily composed of C, N, and O p_z π-type orbitals. Appreciable xanthine C_8 carbon p_π orbital character is found in the HOMO of the neutral 1,7,9-, 1,3,9-, and 1,3,7-xanthine tautomers, and in the LUMO of the 3,7,9-, 1,7,9-, and 1,3,7-xanthine tautomers. The C_8 carbon of xanthine is the locus of nucleophilic attack by metal-activated water in the oxidative hydroxylation of this substrate to uric acid (urate). In orbitally controlled reactions, a large C_8 coefficient in the HOMO may assist in substrate activation via an interaction with the terminal

(81) Maiti, N. C.; Tomita, T.; Kitagawa, T.; Okamoto, K.; Nishino, T. *J. Biol. Inorg. Chem.* **2003**, *8*, 327−333.
(82) Hille, R. *Arch. Biochem. Biophys.* **2005**, *433*, 107−116.

sulfido in XnO_{ox}, while a large coefficient in LUMO facilitates nucleophilic attack on this carbon (vide infra).

Discussion

This work describes a detailed spectroscopic and electronic structure study of the catalytically relevant *cis*-MoOS unit in models for molybdenum hydroxylases. The strong field oxo ligand is known to destabilize the $\psi_{xz,yz}$ π^* orbital set and energetically isolate the ψ_{xy} redox orbital by 13000−16000 cm^{-1} in Mo(V) and Mo(VI) monooxomolybdenum sites. Here, the S K-edge data have been used to calibrate the bonding calculations, which show that the dominant contribution to Mo-S covalency is the π-type (ψ_{xy}) interaction having ∼35% sulfido character. Interestingly, this is more than twice the sulfido character of the σ-type ($\psi_{x^2-y^2}$) orbital (∼15% sulfido character). Thus, an interesting and unusual situation arises in $[MoOS]^{+,2+}$ systems, where π-bond covalency dominates over the σ contribution. Furthermore, the vibrational Raman results indicate that the presence of the sulfido has little effect on the nature of the terminal Mo≡O bond in $[Tp^{iPr}MoOS(OPh)]^{0,-}$, because $\nu_{Mo\equiv O}$ is shifted only slightly from the range of Mo≡O stretching frequencies which have been observed in other monooxomolybdenum compounds. This observation implies that the out-of-plane sulfido orbital, $\chi_{S^{\nu}}$, does not compete favorably with the oxo ligand for the $\psi_{xz,yz}$ orbitals. This is also supported by the S K-edge data and DFT calculations, where it is observed that only ∼22% sulfido character is covalently mixed into ψ_{xz}, ψ_{yz}.

Quantitation of the effective Mo−O_{oxo} and Mo−S bond orders in $[Tp^{iPr}MoOS(OPh)]^{0,-}$ were accomplished using vibrational Raman spectroscopy. The Mo−S force constants (K_{MoS}) were determined for $[Tp^{iPr}MoOS(OPh)]^{0,-}$ and partitioned into their σ and π components, K_σ and K_π, with K_σ being over three times greater than K_π. The Mo−O_{oxo} force constants, K_{MoO}, were determined to be ∼4 times larger than K_{MoS}, consistent with a very strong Mo≡O_{oxo} triple bond, supporting the assertion that the Mo−O_{oxo} bond dominates the ligand field even in the presence of a terminal sulfido donor. With respect to the Mo−S bond in $Tp^{iPr}Mo^{VI}OS(OPh)$, the magnitude of K_{MoS} was found to be consistent with a doubly bonded ($\sigma + \pi$) Mo═S unit. One electron reduction of $Tp^{iPr}Mo^{VI}OS(OPh)$ results in an electron occupying the Mo−S ψ_{xy} π^* orbital, reducing the π-bond order by one-half ($\sigma + 0.5\pi$). In summary, the nature of the bonding in the catalytically essential $[MoOS]^{+,2+}$ unit found in XnO_{ox} and XnO_{vr} has been quantitatively defined, allowing for mechanistic insights into how this moiety is utilized by members of the XnO family in catalysis.

An important issue regarding the role of the Mo−S bond in XnO mediated catalysis relates to the geometric relationship of the $S_{sulfido}$ donor relative to the O_{oxo} and ene-1,2-dithiolate ligands. Several DFT studies have predicted that the most stable geometry for the XnO active site possesses an apical oxo, without a trans ligand, oriented cis to an equatorial sulfido.[83−85] Freeze−quench difference MCD studies of XnO_{vr} provided initial spectroscopic evidence for an apical oxo ligand,[86] and this has been confirmed by an X-ray structure for an inhibitor-bound form of XnO_{red}, which clearly shows the sulfhydryl donor is located in an equatorial position relative to the apical oxo.[1]

The Mulliken population analysis for $Tp^{iPr}Mo^{VI}OS(OPh)$ shows that both the sulfido and oxo donors possess net negative charges, with the magnitude of the O_{oxo} charge dominating, consistent with a more ionic Mo−O_{oxo} bond as compared with Mo−$S_{sulfido}$. The considerable reduction in charge localized on the formally dianionic sulfido ligand is also consistent with the sulfido being a more efficient charge donor to Mo when compared with the O_{oxo} donor. Provided that the sulfido ligand lies in the equatorial plane of the active site under turnover conditions, this geometric arrangement may be anticipated to control the reactivity of the XnO active site with regard to reaction mechanisms involving the sulfido as an electrophile. As such, the bonding description of the *cis*-MoOS unit implicates direct involvement of the sulfido ligand in the reductive half reaction of XnO, providing a potential conduit for electron flow from substrate to the oxidized molybdenum site. During the course of catalysis, electrons will flow from the electron-rich substrate to the electron deficient, XnO_{ox} site. The XnO_{ox} LUMO, which comprises ∼35% $S_{sulfido}$ character, is the likely acceptor orbital in the reduction of the active site molybdenum.

Relationship to the XnO Mechanism. The results of this study allow for an in-depth evaluation of how the unique $[MoOS]^{2+}$ site in XnO_{ox} is engineered to facilitate the two-electron oxidation of purine and aldehyde substrates in the reductive half reaction of the enzyme. Recent studies support a mechanistic proposal that focuses on the transfer of an oxygen atom from metal-activated hydroxide to the substrate.[17,43,44] The proposed water-activation step is similar to that observed in a variety of zinc enzymes, which activate metal-bound water by reducing its pK_a prior to interacting with the substrate.[87,88] By analogy, the high valent $[MoOS]^{2+}$ center in XnO_{ox} is also poised to effectively lower the pK_a of coordinated water facilitating its base-assisted deprotonation. In this way, a coordinated hydroxide is poised for nucleophilic attack on the C_8 position of xanthine or the analogous carbon atom of alternative substrates. Computational studies have identified a transition state in the reaction of the simple substrate, formamide, with XnO_{ox}.[85] The calculated electron density change at the transition state, relative to the reactants, indicates that the initial nucleophilic attack is followed by hydride transfer to $S_{sulfido}$, with the obligatory catalytic intermediate being a product bound, Mo−$OR_{product}$, complex.[85] This idea is supported by a very elegant ^{13}C ENDOR study on XnO_{vr} that showed that the calculated Mo−C_8 distances are consistent with a Mo−$OR_{product}$ species, likely bound as the enolate tautomer.[25]

The results of our spectroscopic studies and bonding calculations show that the catalytically relevant XnO_{ox} LUMO (ψ_{xy}) is effectively heteronuclear diatomic in nature[89] and highly delocalized over both the Mo and S atoms in a manner that is remarkably similar to the Cu−S_{cys} interaction in blue copper

(83) Bray, M. R.; Deeth, R. J. *Inorg. Chem.* **1996**, *35*, 5720−5724.
(84) Bray, M. R.; Deeth, R. J. *J. Chem. Soc., Dalton Trans.* **1997**, 1267−1268.
(85) Ilich, P.; Hille, R. *J. Phys. Chem. B* **1999**, *103*, 5406−5412.
(86) Jones, R. M.; Inscore, F. E.; Hille, R.; Kirk, M. L. *Inorg. Chem.* **1999**, *38*, 4963−4970.
(87) Banci, L.; Bertini, I.; Lapenna, G. *Proteins: Struct. Funct. Genet.* **1994**, *18*, 186−197.
(88) Greene, D.; Das, B.; Fricker, L. D. *Biochem. J.* **1992**, *285*, 613−618.
(89) The description of the LUMO wavefunction as heteronuclear diatomic stems from the fact that the dominant component of the wavefunction (>80%) is localized on the molybdenum and sulfido sulfur atoms.

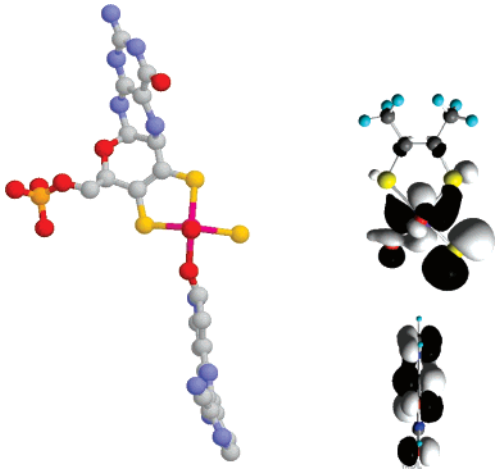

Figure 6. Left: X-ray structure of the XnO-FYX-051 inhibitor bound species;[1] Right: proposed encounter complex orientation between the XnO active site LUMO and the xanthine HOMO: (Mo) magenta; (S) yellow; (O) red; (N) blue. Note that the structure on the right has been rotated ~45° relative to the structure on the left.

proteins.[90,91] This energetic isolation (~1 eV) of the ψ_{xy} antibonding orbital from the rest of the Mo d orbital manifold defines it as the electron acceptor orbital, and the large Mo−$S_{sulfido}$ covalency in XnO_{ox} results in the $S_{sulfido}$ being considerably more electrophilic than the terminal oxo. This is reflected in the calculated Mulliken charges of $S_{sulfido}$ and O_{oxo} in the computational $[MoOS]^{2+}$ models as well as computational models for XnO_{ox}. With respect to the O_{oxo} donor, the more electrophilic nature of $S_{sulfido}$ in the $[MoOS]^{2+}$ unit is consistent with a formal hydride transfer mechanism, with $S_{sulfido}$ acting as hydride acceptor. This formal description of the reactivity implies heterolytic C_8−H bond cleavage. However, our understanding of the ψ_{xy} XnO_{ox} LUMO provides further insight into this crucial idea and allows for various symmetry and orbital aspects to be considered in the mechanism.

Inspection of the inhibitor orientation in the structure of XnO-FYX-051 (Figure 6) provides some additional clues regarding the intimate details of the reductive half reaction. It is observed here that the inhibitor is oriented in the active site with the aromatic ring and the apical Mo−O_{oxo} bond vector in the same plane.[1] An analogous situation is observed in the crystal structures of the XnO−alloxanthine[15] complex and the salicylate bound form of *R. capsulatus* XDH. Provided that XnO_{ox} possesses an apical O_{oxo} oriented cis to an equatorial $S_{sulfido}$, the encounter geometry is similar to that proposed by Hille et al.[85] This is important, as this active site orientation places the $\chi_{S^{\pi}}$ orbital, that comprises a large portion of the ψ_{xy} π^* LUMO, in the same plane as the C_8 p_{π} orbital of the native xanthine substrate, poised for maximum π^* LUMO−C_8 p_{π} orbital overlap. The concept of charge and frontier orbital controlled reactions describes how such orientational effects can play a significant role in chemical reactivity, particularly in facilitating the hydroxylation of xanthine and other aromatic heterocyclic substrates. The relevant equation for the total perturbation energy of the reaction is given by eq 5.[92]

$$\Delta E_{tot} = \frac{-q_{sulfido}q_{C8}}{R\epsilon} + \frac{2c_{S\pi^*}{}^2 c_{C8p}{}^2 \beta^2}{E_{Xn\cdot HOMO} - E_{XnO\cdot LUMO}} \qquad (5)$$

This describes the charge and orbital dependence on the initial slope of the reaction pathway toward the transition state. In the first term, $q_{sulfido}$ is the charge on the sulfido ligand in XnO_{ox} and q_{C8} is the charge on the C_8 carbon of xanthine. The parameter R is the distance between the sulfido ligand and the C_8 carbon, and ϵ is the local dielectric constant. The molecular orbital coefficients for $S_{sulfido}$ in the XnO_{ox} LUMO, and C_{8p} in the xanthine HOMO, along with the resonance integral, β, are found in the numerator of the second term in eq 5, and the energy difference between the XnO_{ox} LUMO and the xanthine HOMO comprises the denominator.

When the energy difference between the HOMO and LUMO is much greater than $2c_i^2c_j^2\beta^2$, the first term in eq 5 dominates, and the reaction is said to be charge controlled. However, under conditions where this energy difference is small, the second term dominates and the reaction is orbitally controlled. Since the magnitudes of the calculated charges on $S_{sulfido}$ and the C_8 of xanthine are small, the hydroxylation of xanthine is anticipated to be under orbital control. As the geometry of the encounter complex plays a dominant role in orbitally controlled reactions, maximal orbital overlap between the Mo=S π^* LUMO and the C_8 p orbital of the xanthine HOMO is favored to facilitate a charge transfer from xanthine to XnO_{ox}. Our calculations show that $c_{S\pi^*}{}^2 = 0.35-0.40$, while c_{C8p^2} for xanthine is ~0.08, and the maximum orbital interaction is achieved when the C_8 p orbital approaches the active site in the equatorial (*xy*) plane (Figure 6). The initial step in the reaction may therefore be the formation of relatively weak σ-type overlap between the C_8 carbon p_{π} orbital and the $\chi_{S^{\pi}}$ sulfido p-orbital. This interaction would be anticipated to polarize the C_8 carbon of substrate, increasing its electrophilicity and activating the substrate for nucleophilic attack by the metal- bound hydroxide. The resultant negative charge accumulation on the purine ring following hydroxide attack could then break down by formal hydride transfer, with the trajectory of the C_8 hydrogen toward the terminal sulfido ligand.

The mechanisms above involve nucleophilic attack of metal-activated hydroxide on the C_8 carbon of xanthine or the carbonyl carbon of aldehyde and amide substrates. These mechanisms tacitly assume the transfer of the metal-bound hydroxide to the substrate carbon *without the formation of a substrate-bound intermediate.* Key to this mechanistic sequence is the heterolytic scission of the substrate C−H bond and transfer of hydride to the ψ_{xy} π^* acceptor orbital of the sulfido ligand. Thus, the ψ_{xy} π^* orbital plays the role of dual electron acceptor. Two important caveats must be mentioned at this point regarding a hydride transfer mechanism. First, the terminal sulfido ligand in XnO_{ox} possesses a small net *negative charge*, reducing the driving force for hydride transfer to this atomic center via a charge controlled process. Second, attack of metal-bound hydroxide on the purine or carbonyl carbon of substrate should lead to immediate deprotonation of the hydroxide yielding a

(90) Palmer, A. E.; Randall, D. W.; Xu, F.; Solomon, E. I. *J. Am. Chem. Soc.* **1999**, *121*, 7138−7149.
(91) Randall, D. W.; deBeer George, S.; Holland, P. L.; Hedman, B.; Hodgson, K. O.; Tolman, W. B.; Solomon, E. I. *J. Am. Chem. Soc.* **2000**, *122*, 11632−11648.
(92) Bersuker, I. B. *Electronic Sturcture and Properties of Transition Metal Compounds. Introduction to the Theory*; Wiley-Interscience: New York, 1996.

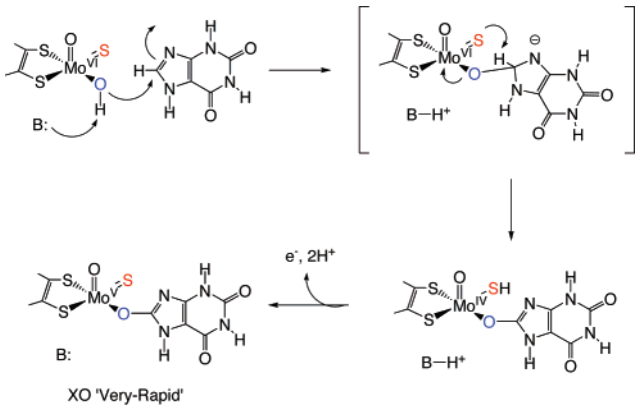

Figure 7. Modified hydride transfer mechanism described as an inner sphere electron-transfer mediated by the Mo−OR bond concomitant with *proton* transfer to the terminal sulfido. The mechanism shows that through-bond electron-transfer coupled to C−H bond scission and proton transfer to the terminal sulfido represents a coupled 2-electron proton-transfer description of formal hydride transfer. Here, B: is the general base Glu 1261.

Mo−OR intermediate (Figure 7). This bonding scheme has been observed in the recent X-ray structure of the XnO-FYX-051 bound species.[1] Here, the hydride transfer may alternatively be described as an inner sphere electron-transfer mediated by the Mo−OR bond concomitant with *proton* transfer to the terminal sulfido ligand. Partial or complete two-electron reduction of the Mo center at the transition state would render the sulfido a powerful proton acceptor (nucleophile). To the extent that the through bond electron transfer is coupled to C−H bond scission and proton transfer to the terminal sulfido, this represents an unusual example of a coupled 2-electron proton transfer.[93]

A number of key factors appear to have a significant effect on accelerating the rate of substrate oxidation by molybdenum hydroxylases. First, the high-valent Mo center plays a role similar to that found in non-redox active metallohydrolase enzymes. Here, water is activated for nucleophilic attack on substrate via its deprotonation. Second, the redox component of catalysis likely occurs after nucleophilic attack of metal activated water on the substrate, and the ψ_{xy} π^* orbital acts as the two electron acceptor orbital in either a hydride or coupled $2e^-/H^+$ transfer mechanism. Finally, in each of the models presented the substrate binding pocket serves a very important role in orienting the substrate for enzymatic hydroxylation and may further aid in regioselectivity.[94] Ongoing work is focussed on utilizing simple, alternative substrates to delineate the differences between formal hydride and various coupled e^-/H^+ transfer mechanisms for the breakdown of the proposed intermediate/transition state. However, it must be recognized that the oxidative hydroxylation of amides and aldehydes, which are alternative substrates for XnO, may be different from that of aromatic heterocycles resulting in a substrate dependent reaction mechanism.

(93) Brunold, T. C.; Solomon, E. I. *J. Am. Chem. Soc.* **1999**, *121*, 8288−8295.

Summary

The electronic structure of the *cis*-MoOS unit has been studied in detail using S K-edge XAS and vibrational spectroscopies coupled with detailed bonding calculations, and the results have been used to gain additional insight into the mechanism of XnO. A strong covalent interaction between Mo and the terminal sulfido ligand results in a highly delocalized LUMO (ψ_{xy}) that has been hypothesized to play a role in polarizing a substrate carbon center for nucleophilic attack by metal activated water and acting as an electron sink in the two-electron oxidation of the substrate. Interestingly, members of the XnO family appear to be unique among enzymes in their ability to activate both water and substrate to catalyze substrate hydroxylation reactions.

Acknowledgment. M.L.K. acknowledges the National Institutes of Health (Grant GM-057378) for financial assistance. C.G.Y. thanks Dr. P. D. Smith for experimental assistance and gratefully acknowledges the financial support of the Australian Nuclear Science and Technology Organization (for travel to S.S.R.L.), the Australian Research Council, and the donors of the Petroleum Research Fund (administered by the American Chemical Society). Portions of this work were carried out at the Stanford Synchrotron Radiation Laboratory which is funded by the U.S. DOE, BES, and OBES, and the NIH, NCRR. Work at the University of Saskatchewan was supported by a Canada Research Chair award (G.N.G.).

Supporting Information Available: Complete ref 57; Mo L_2-edge spectrum (Figure S1); room-temperature electronic absorption spectrum of $CoCp_2[Tp^{iPr}MoOS(OPh)]$ in acetonitrile (Figure S2). This material is available free of charge via the Internet at http://pubs.acs.org.

JA068512M

(94) Rastelli, G.; Costantino, L.; Albasini, A. *J. Am. Chem. Soc.* **1997**, *119*, 3007−3016.